International Journal of Heat and Mass Transfer 263 (2026) 128560

Contents lists available at ScienceDirect

International Journal of Heat and Mass Transfer

journal homepage: www.elsevier.com/locate/ijhmt

Diffusion measurements of Si in liquid Al-Cu-Si alloy using X-ray radiography and shear cell techniques

Masato Shiinoki [a,b,*], Elke Sondermann [c], Andreas Meyer [c], Shinsuke Suzuki [a,b,d]

[a] Department of Applied Mechanics and Aerospace Engineering, Faculty of Science and Engineering, Waseda University, Okubo 3-4-1 Shinjhuku-ku, 169-8555 Tokyo, Japan
[b] Kagami Memorial Research Institute of Materials Science and Technology, Waseda University, Nishiwaseda 2-8-26 Shinjuku-ku, 169-0051 Tokyo, Japan
[c] Institut für Materialphysik im Weltraum, Deutsches Zentrum für Luft- und Raumfahrt (DLR), Linder Höhe, 51170 Köln, Germany
[d] Department of Materials Science, Graduate School of Fundamental Science and Engineering, Waseda University, Okubo 3-4-1 Shinjuku-ku, 169-8555 Tokyo, Japan

ARTICLE INFO

Keywords:
Diffusion coefficient
X-ray radiography
Shear cell technique
Stable density layering
ICP-OES
Al-Cu-Si
Thermodynamic factor

ABSTRACT

Impurity diffusion coefficients of Si in liquid Al alloys are essential for understanding solidification but are difficult to measure due to convection and the ineffectiveness of X-ray radiography (XRR) for elements with similar atomic numbers. To address this problem, this study aims to propose a methodology for determining diffusion coefficients by using a tracer to quantify and correct for additional mass transport. Diffusion experiments were conducted on Al-Cu-Si alloys at 973 K, combining XRR and the shear cell techniques with stable density layering by adding Cu to the Al-Si system. Using Cu as a tracer allowed for the quantitative evaluation of shear convection via in-situ XRR. Based on the impurity diffusion coefficients of Cu obtained from XRR results, it was confirmed that the diffusion experiments were conducted under conditions where natural convection was effectively suppressed during the entire diffusion time. Furthermore, the additional mass transport induced by shear convection was quantitatively corrected by isolating the initial mass transport from cell insertion and the final mass transport from cell separation. The initial mass transport was derived from the intercept of in-situ XRR data. The final mass transport was determined by the difference between the final XRR and inductively coupled plasma optical emission spectroscopy (ICP-OES) results for Cu. The obtained impurity diffusion coefficient of Si was determined to be $(7.81 \pm 0.90) \times 10^{-9}$ m^2s^{-1} at 973 K. Additionally, the validity of adding Cu was confirmed by thermodynamic calculations, which showed that the thermodynamic coupling between Cu and Si fluxes in the ternary system is negligible.

1. Introduction

Diffusion coefficients in liquid metals are essential for understanding metallurgical phenomena and developing diffusion models. Furthermore, impurity diffusion coefficients in the liquid phase are required for solute redistribution at the solid-liquid interface during solidification process where alloys are often formed between elements with similar atomic numbers [1,2]. For example, Al-Si alloys are widely used in industrial castings such as engine blocks. However, reliable impurity diffusion data for liquid metals is limited because impurity diffusion measurements with high precision are hindered by natural convection on the ground or uncertainties in concentration analysis. To address this issue, in-situ measurement of concentration profiles in the liquid state using X-ray radiography (XRR) [3–5] or X-ray fluorescence analysis [6, 7] effectively eliminates the influence of concentration changes during solidification. Additionally, the shear cell [8] and sliding cell techniques [9], which mechanically separate the diffusion couple prior to solidification, mitigates such effects. Suppressing natural convection with a stable density layering [8], in which the density of the diffusion couple increases monotonically in the direction of gravity, has proven effective.

However, the Al–Si system, which has similar atomic numbers, remains challenging for measuring impurity diffusion coefficients, even when using the above-described methods. Although limited data exist, such as the work by Kikuchi et al. [10], impurity diffusion coefficients of Si in liquid Al were often measured using conventional methods like the capillary reservoir technique. These methods are susceptible to natural convection, leading to scattered or overestimated diffusion coefficients. Therefore, a rigorous remeasurement using a convection-suppressed method is indispensable to establish reliable reference data. In the

* Corresponding author.
E-mail addresses: stag7211@asagi.waseda.jp (M. Shiinoki), Elke.Sondermann@dlr.de (E. Sondermann), Andreas.Meyer@dlr.de (A. Meyer), suzuki-s@waseda.jp (S. Suzuki).

https://doi.org/10.1016/j.ijheatmasstransfer.2026.128560
Received 14 November 2025; Received in revised form 25 January 2026; Accepted 15 February 2026
Available online 9 March 2026
0017-9310/© 2026 The Authors. Published by Elsevier Ltd. This is an open access article under the CC BY license (http://creativecommons.org/licenses/by/4.0/).

Nomenclature

c_i	Concentration of impurity element i (at %)
c_0	Initial concentration of impurity in semi-infinite sample (at %)
$D_{app(Cu)}$	Apparent impurity diffusion coefficient of Cu ($m^2\ s^{-1}$)
D_{Si}	Impurity diffusion coefficient of Si ($m^2\ s^{-1}$)
D_{ref}	Referenced diffusion coefficient ($m^2\ s^{-1}$)
$[D]$	Diffusion coefficient matrix ($m^2\ s^{-1}$)
g	Gravity vector ($m^2\ s^{-1}$)
G_{ex}	Excess Gibbs free energy (J mol^{-1})
G_{ideal}	Ideal mixing Gibbs free energy (J mol^{-1})
G_m	Molar Gibbs free energy (J mol^{-1})
G_{ref}	Reference Gibbs free energy (J mol^{-1})
$\Gamma_{\alpha\beta}$	Thermodynamic factor between components α and β (-)
$[\Gamma]$	Thermodynamic factor matrix (-)
h_0	Initial thickness of an intermediate cell (m)
$[H_{\alpha\beta}]$	Hessian matrix between components α and β (-)
L_{mn}	Binary interaction parameter of Redlich-Kister polynomial expansion between components m and n (J mol^{-1})
${}^{(l)}L_{mn}$	l-th order binary interaction parameter (J mol^{-1})
$L_{Al,Cu,Si}$	Ternary interaction parameter of Redlich-Kister polynomial expansion for the Al-Cu-Si system (J mol^{-1})
$[M]$	Mobility matrix ($m^2\ s^{-1}$)
N	Molar fraction (-)
R	Gas constant (J $mol^{-1}\ K^{-1}$)
R^2	Coefficient of determination (-)
t	Time elapsed since the start of diffusion (s)
t_{diff}	Diffusion time (s)
T	Temperature (K)
U_{aver}	Uncertainty of $\langle X^2_{aver}\rangle$ (m^2)
$U(D_{Si})$	Uncertainty of D_{Si} ($m^2\ s^{-1}$)
U_{ICP_Si}	Uncertainty of $\langle X^2_{meas}\rangle_{ICP\_Si}$ (m^2)
$U_{shear\ out\ +\ aver}$	Uncertainty of $\langle X^2_{shear\ out}\rangle + \langle X^2_{aver}\rangle$ (m^2)
$U_{shear\ in}(t_{diff})$	Uncertainty of $\langle X^2_{shear\ in}\rangle$ at t_{diff} (m^2)
x	Position (m)
x_0	Initial position of the interface of the diffusion couple (m)
$\langle X^2_{aver}\rangle$	Additional mean-square diffusion depth resulting from plot of average value for each cell (m^2)
$\left\langle X^2_{diff}(t)\right\rangle$	Mean-square diffusion depth contributed from diffusion at t (m^2)
$\langle X^2_{meas}(t)\rangle_{j\text{-}i}$	Measured mean-square diffusion depth for impurity i using analysis method j at t (m^2)
$\langle X^2_{shear\ out}\rangle$	Additional mean-square diffusion depth during the separation of the cell at the end of the diffusion process (m^2)
$\langle X^2_{shear\ in}\rangle$	Additional mean-square diffusion depth during the insertion of the intermediate cell in the shear cell (m^2)

Subscripts

i	Impurity element (in this study : Cu or Si)
j	Analysis method for the impurity concentration (in this study : XRR or ICP)
α, β	Components for the thermodynamic factor (in this study : Cu or Si)
m, n	Components for the binary interaction parameter of Redlich-Kister polynomial expansion (in this study : Al, Cu, or Si)

Superscripts

l	Order of the Redlich-Kister binary interaction parameter (-)

case of impurity diffusion of Si in liquid Al alloys, the slight density difference between Al and Si makes it difficult to achieve the stable density layering. Additionally, in-situ concentration analysis of Si is hindered by its characteristic X-ray intensity being comparable to that of Al, which makes it impractical to accurately assess natural convection suppression or determine solute concentration profiles. Furthermore, Si is a poorly soluble substance in acid. While Si can be dissolved using hydrofluoric acid, the resulting volatility at high temperatures renders the solute difficult to handle. To overcome these challenges, the present study focuses on Cu, an impurity element for which reliable diffusion data in liquid Al alloys is available [11]. Adding Cu to the Al-Si system achieves stable density layering because a heavy element serves as an anchor. This method is similar to adding Bi to Sn-In [12] or Ag to Pb isotopes [13] in the diffusion experiments. In-situ concentration profiles of Cu are obtained using XRR, enabling direct verification of the suppression of natural convection. The Si concentration profile was obtained by inductively coupled plasma optical emission spectroscopy (ICP-OES) on samples collected after the shear cell technique. To prevent the volatilization of Si during hydrofluoric acid dissolution, the diffusion samples with Si are dissolved in sealed containers. However, even with accurate concentration analysis, mechanical operations in the shear cell technique inevitably introduce additional mass transport, specifically shear convection [8,14], which can lead to overestimated diffusion coefficients. Crucially, the use of Cu as a visible tracer enables the quantitative evaluation of this additional mass transport through in-situ XRR. This quantification allows for the mathematical correction of the Si concentration profiles obtained from post-mortem analysis, ensuring the isolation of the true diffusive component. Therefore, the impurity diffusion coefficient in the Al–Si system, which has traditionally been difficult to determine, is measured by combining the XRR and shear cell techniques.

The objective is to propose a methodology for determining diffusion coefficients by using a tracer to quantify and correct for additional mass transport. Diffusion experiments were conducted on Al-Cu-Si alloys at 973 K, just above the melting point of Al, combining XRR and shear cell techniques. In this setup, stable density layering was achieved by adding Cu to the Al-Si system. The impurity diffusion coefficient of Cu was calculated from the XRR results and compared with previously reported values [11] where natural convection suppression had been confirmed to verify suppression of convection in this system. Furthermore, comparing the mean-square diffusion depth (MSD) of Cu in liquid Al obtained by XRR and ICP enables the quantification of additional mass transport induced by the shear convection, which is unique to the shear cell technique, as detailed in Section 2. Finally, correcting for this quantified shear convection using MSD when calculating the impurity diffusion coefficient of Si in liquid Al yielded a precision value. To supplement this methodology, this study also investigates the thermodynamic coupling in the ternary Al-Cu-Si system, validating that the influence of the Cu tracer on the Si diffusional flux is minimal.

2. Analysis model

In this study, the shear cell technique was employed to measure impurity diffusion coefficients in liquid metals. In this specific study, a diffusion couple was formed by contacting pure Al with an Al-Cu-Si alloy within a capillary. Accurate determination of the diffusion coefficient requires accounting for additional mass transport caused by the shear cell operation. Specifically, friction between the liquid and the moving

disk induces the "shear convection" [8,14]. This section describes the model used to quantify the impact of additional mass transport and to isolate the purely diffusive contribution using the MSD, denoted as $\langle X^2 \rangle$.

The quantification of this shear convection is realized based on the following concept, utilizing Cu as a tracer. Figs. 1 and 2 show the schematics of analysis procedure and of time-resolved MSD of Cu and Si, respectively. First, the process for Cu, which serves as a tracer with X-ray contrast, is described. In the initial setup before the diffusion process, as shown in Fig. 1(a), the diffusion couple is separated. Then, at the start of the diffusion process at time $t = 0$, the insertion of the intermediate cell induces shear convection, as depicted in Fig. 1(c). After starting the diffusion process, the concentration profile is described by the analytical solution of Fick's second law for this geometry. Eq. (1) expresses this relationship:

$$c_i(x,\ t) = \frac{c_0}{2}\left\{1 - \mathrm{erf}\left(\frac{x - x_0}{\sqrt{2\langle X^2_{\mathrm{meas}}(t)\rangle_{j-i}}}\right)\right\}. \tag{1}$$

Here, $c_i(x)$ is the concentration of impurity element i at a position x in the capillary, c_0 is the initial concentrations of the impurity element in the alloy sample, x_0 is the initial position of the interface of the diffusion couple, and $\langle X^2_{\mathrm{meas}}(t)\rangle_{j\text{-}i}$ is the measured MSD at t for impurity i using the analysis method j (XRR or ICP). The parameters mentioned above are schematically illustrated in Fig. 1(a) and (b). Then, at the start of the diffusion process at $t = 0$, the insertion of the intermediate cell induces a mechanical disturbance, referred to here as shear convection, as depicted in Fig. 1(c). This mass transport broadens the concentration profile,

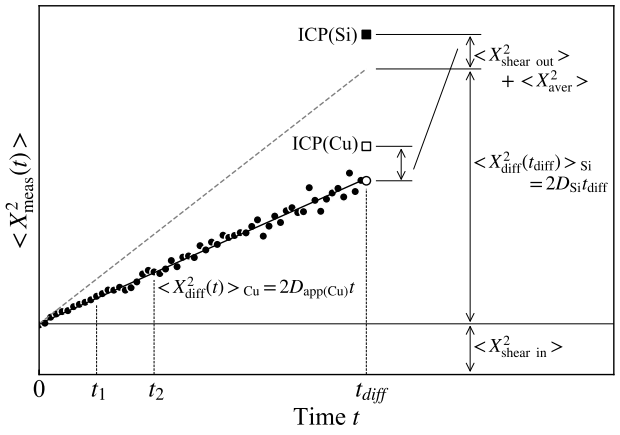

Fig. 2. Schematics of time-resolved MSD of Cu and Si with $\langle X^2_{\mathrm{aver}}\rangle$, $\langle X^2_{\mathrm{meas}}\rangle$, $\langle X^2_{\mathrm{diff}}\rangle$, $\langle X^2_{\mathrm{shear\ in}}\rangle$, and $\langle X^2_{\mathrm{shear\ out}}\rangle$ during the diffusion process for the analysis model. The symbol D means impurity diffusion coefficient. The black plots are $\langle X^2_{\mathrm{meas}}(t)\rangle_{\mathrm{XRR\_Cu}}$. The open circle is the MSD at the end of the diffusion process $t = t_{\mathrm{diff}}$. The open and black squares are $\langle X^2_{\mathrm{meas}}(t_{\mathrm{diff}})\rangle_{\mathrm{ICP\_Cu}}$ and $\langle X^2_{\mathrm{meas}}(t_{\mathrm{diff}})\rangle_{\mathrm{ICP\_Si}}$, respectively. The solid and dashed lines are linear fit of $\langle X^2_{\mathrm{meas}}(t)\rangle_{\mathrm{XRR\_Cu}}$ and eye-guide line of $\langle X^2_{\mathrm{meas}}\rangle$ of Si, respectively. This dashed line conceptually illustrates the assumption that the purely diffusive component of Si behaves linearly with time, parallel to that of Cu. The times t_1, t_2 and t_{diff} correspond to the times shown in Fig. 1.

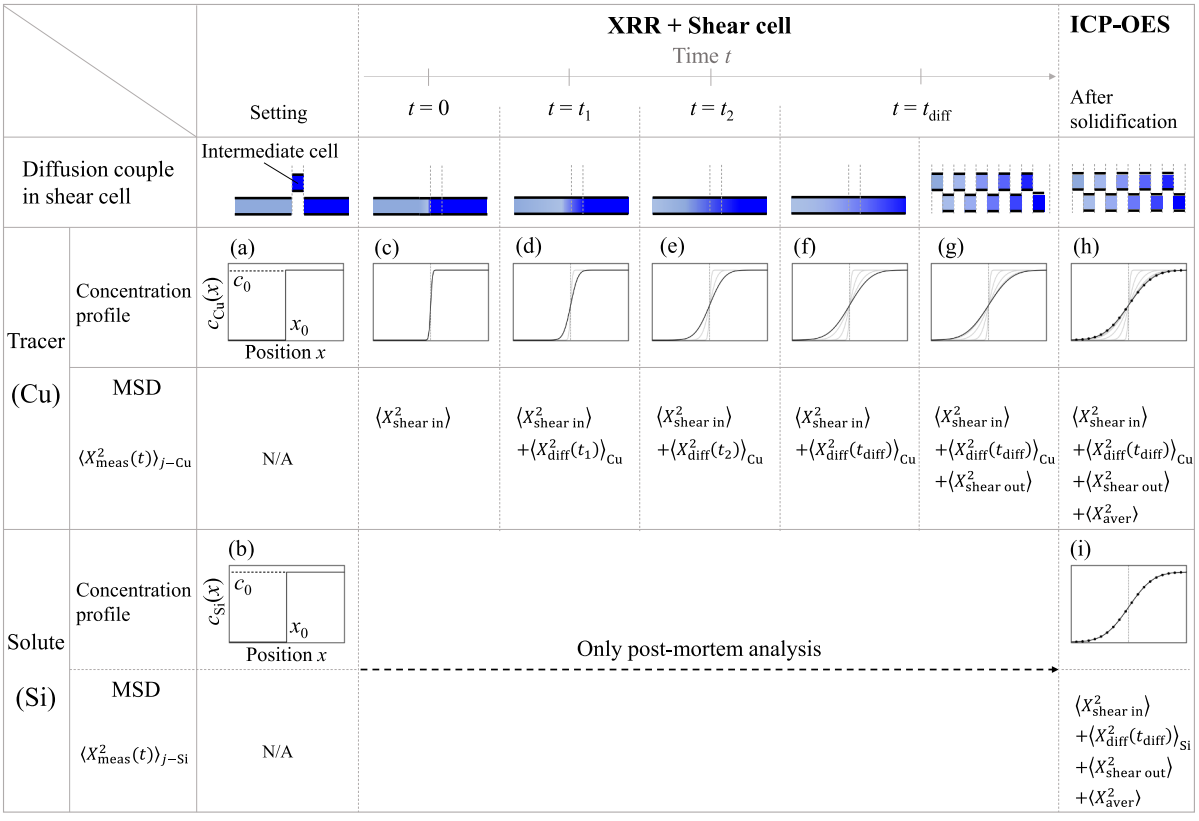

Fig. 1. Schematics of analysis procedure combining XRR, shear cell, and ICP-OES. The symbol t means the time elapsed since the start of diffusion and the subscript j on $\langle X^2_{\mathrm{meas}}\rangle$ means the analysis method for the impurity concentration (in this study : XRR or ICP). (a) and (b) concentration profiles of Cu and Si in setting before the diffusion process, respectively, (c) start of the diffusion process by inserting the intermediate cell at $t = 0$, (d) and (e) diffusion processes at $t = t_1$ and t_2, respectively, (f) end of the diffusion process at $t = t_{\mathrm{diff}}$ before shearing the cells, (g) end of the diffusion process at $t = t_{\mathrm{diff}}$ after shearing the cells, and (h) and (i) concentration profiles of Cu and Si after cooling, respectively.

and the initial measured MSD, $\langle X^2_{\mathrm{meas}}(0)\rangle_{\mathrm{XRR\_Cu}}$, corresponds to $\langle X^2_{\mathrm{shear\ in}}\rangle$. This value is plotted at $t = 0$ in Fig. 2. As the diffusion process proceeds to times t_1 and t_2 (Fig. 1(d) and (e)), the concentration profile of Cu further broadens by an amount corresponding to $\left\langle X^2_{\mathrm{diff}}(t_1)\right\rangle$ or $\left\langle X^2_{\mathrm{diff}}(t_2)\right\rangle$, respectively. At these points, $\langle X^2_{\mathrm{meas}}(t)\rangle_{\mathrm{XRR\_Cu}}$ is the sum of $\langle X^2_{\mathrm{shear\ in}}\rangle$ and $\left\langle X^2_{\mathrm{diff}}(t)\right\rangle$, which are plotted at $t = t_1$ and t_2 in Fig. 2. This measured MSD is expected to follow the linear relationship. The apparent impurity diffusion coefficient of Cu, $D_{\mathrm{app(Cu)}}$, was determined from the slope of the linear fit to time, as expressed in Eq. (2) .

$$\langle X^2_{\mathrm{meas}}(t)\rangle_{\mathrm{XRR\_Cu}} = \langle X^2_{\mathrm{shear\ in}}\rangle + 2D_{\mathrm{app(Cu)}}t. \tag{2}$$

Consequently, the slope of $\langle X^2_{\mathrm{meas}}(t)\rangle_{\mathrm{XRR\_Cu}}$ in Fig. 2 corresponds to $2D_{\mathrm{app(Cu)}}$. The diffusion process continues until the designated diffusion time, t_{diff} (Fig. 1(f)). The $\langle X^2_{\mathrm{meas}}(t)\rangle_{\mathrm{XRR\_Cu}}$ just before the shear cell separation is plotted as an open circle at $t = t_{\mathrm{diff}}$ in Fig. 2. Upon separation of the shear cell, the resulting mass transport further broadens the concentration profile, an effect quantified as $\langle X^2_{\mathrm{shear\ out}}\rangle$ (Fig. 1(g)). At this stage, $\langle X^2_{\mathrm{meas}}(t_{\mathrm{diff}})\rangle_{\mathrm{XRR\_Cu}}$ becomes the sum of $\langle X^2_{\mathrm{shear\ in}}\rangle$, $\left\langle X^2_{\mathrm{diff}}(t_{\mathrm{diff}})\right\rangle$, and $\langle X^2_{\mathrm{shear\ out}}\rangle$. As shown in Fig. 1(h), each sample is cooled to room temperature and subsequently analyzed by ICP-OES. The $\langle X^2_{\mathrm{meas}}(t_{\mathrm{diff}})\rangle_{\mathrm{ICP\_Cu}}$ obtained by fitting the diffusion equation to the ICP-derived concentration profile includes an additional term, $\langle X^2_{\mathrm{aver}}\rangle$, which accounts for the apparent geometric progression of diffusion due to cell segmentation [8]. Thus, the final $\langle X^2_{\mathrm{meas}}(t_{\mathrm{diff}})\rangle_{\mathrm{ICP\_Cu}}$ is the sum of $\langle X^2_{\mathrm{shear\ in}}\rangle$, $\left\langle X^2_{\mathrm{diff}}(t_{\mathrm{diff}})\right\rangle$, $\langle X^2_{\mathrm{shear\ out}}\rangle$, and $\langle X^2_{\mathrm{aver}}\rangle$, which is plotted as an open square in Fig. 2. Consequently, the combined value of $\langle X^2_{\mathrm{shear\ out}}\rangle + \langle X^2_{\mathrm{aver}}\rangle$ can be determined by subtracting the value of the open circle from that of the open square.

Next, the process for Si is explained. As with Cu, the diffusion couple for Si is initially separated (Fig. 1(b)). However, the concentration of Si in liquid Al provides no contrast in XRR and thus cannot be monitored in-situ. The concentration profile of Si is obtained solely from the post-mortem ICP-OES analysis. The measured $\langle X^2_{\mathrm{meas}}(t_{\mathrm{diff}})\rangle_{\mathrm{ICP\_Si}}$ from this analysis is considered to be the sum of all components: $\langle X^2_{\mathrm{shear\ in}}\rangle$, $\left\langle X^2_{\mathrm{diff}}(t_{\mathrm{diff}})\right\rangle$, $\langle X^2_{\mathrm{shear\ out}}\rangle$, and $\langle X^2_{\mathrm{aver}}\rangle$. To isolate the purely diffusive component, $\left\langle X^2_{\mathrm{diff}}(t_{\mathrm{diff}})\right\rangle$, for Si, the convective components determined using the Cu tracer—namely $\langle X^2_{\mathrm{shear\ in}}\rangle$ and the combined $\langle X^2_{\mathrm{shear\ out}}\rangle + \langle X^2_{\mathrm{aver}}\rangle$—are subtracted from the total measured value for Si, as illustrated in Fig. 2. This procedure enables the calculation of the impurity diffusion coefficient of Si, corrected for the effects of shear convection.

3. Experimental procedure

Al (99.999 at % purity; Alfa Aesar GmbH & Co KG), Cu (99.99 at % purity; Alfa Aesar GmbH & Co KG), and Si (99.999 at % purity; Alfa Aesar GmbH & Co KG) were used as raw materials to prepare diffusion samples. Al-Cu-Si diffusion samples were prepared as follows: the impurity element contents were 5 at % for Cu and 5 at % for Si. Each pure metal sample was weighed to obtain the desired concentration, as described above. The metals were melted using an arc-melting furnace (MAM-1, Edmund Bühler GmbH). The arc current was adjusted to heat the sample above 1773 K, ensuring the complete fusion of Si, which has the highest melting point. Subsequently, the molten alloy was poured into a water-cooled copper mold. Two types of molds were prepared, with diameters of 1.4 mm and 3.0 mm, respectively. Finally, the samples were cut to fit the diffusion capillaries. Additionally, the absence of severe solidification segregation in the prepared samples was verified using X-ray radiography images.

Fig. 3 shows a schematic illustration of the experimental procedure for the shear cell technique. The detailed design and procedures of the diffusion experiments can be found in previous experiments [15]. The two capillaries were labelled Capillaries A and B. The experiment consisted of the diffusion process between two semi-infinite samples: one composed of an Al-Cu-Si alloy and the other of pure Al. The diffusion temperature was 973 K, and the t_{diff} during the experiments was 860 s.

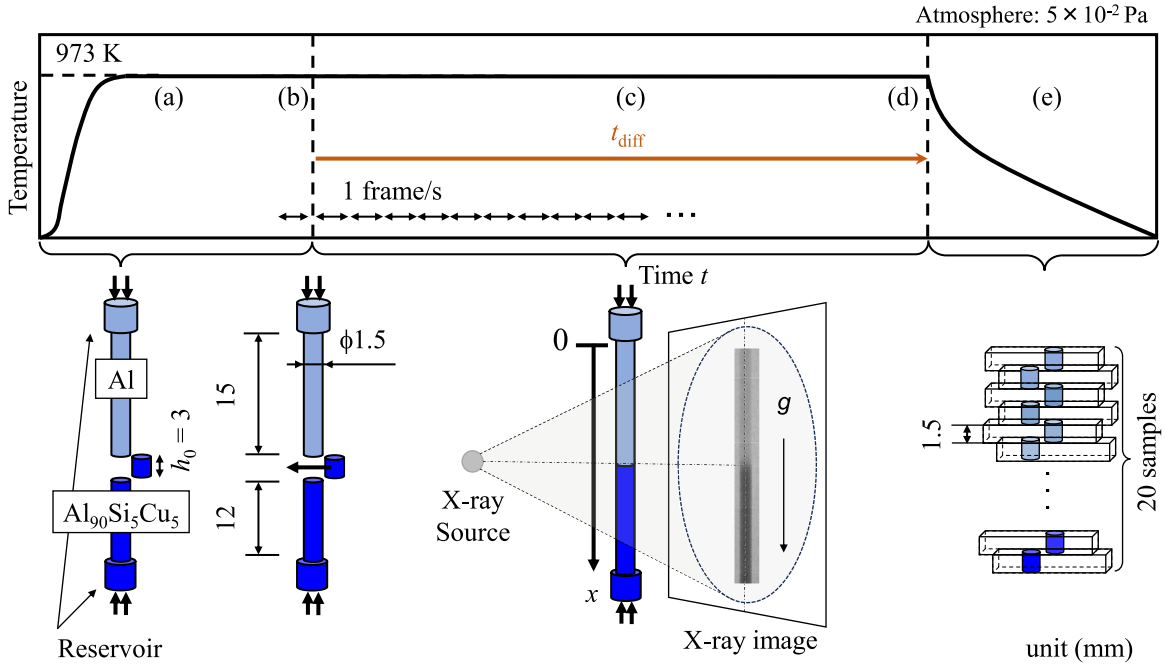

Fig. 3. Schematic illustration of experimental procedure of the shear cell technique, which indicates one of the two capillaries as an example: (a) heating and homogenization, (b) insertion set at $t = 0$, (c) diffusion process with the XRR, (d) separation of sample at end of diffusion process at $t = t_{\mathrm{diff}}$, and (e) cooling. The symbol h_0 is the initial thickness of the alloy cell. The capillary was set so that the gravity vector g would be parallel to it. The double arrows from (b) to (c) indicate the XRR exposure time, with exposures of 1 frame/s intervals.

When the samples were set into the shear cell device, the higher-density samples of the Al-Cu-Si alloy were placed on the lower side to obtain stable density layering. Reservoir samples were set using elastically compressed graphite felts. The shear cell device, heater, and motor were placed in a vacuum chamber. For X-ray imaging, a micro-focus X-ray source (XT9160-TED, Viscom AG), operating at 150 kV and 250 μA, and a 2 mm CdTe detector with a 100 μm pixel size (XC-Thor, Direct Conversion AB) was used. The effective pixel size for the experiment was about 50 μm. The sample cell was located between the source and the detector. The images were filtered by flat-field correction with reference gray images.

After homogenization for 3600 s, the intermediate cell was inserted into each capillary, and the diffusion process was started. At this time, t was set to 0. X-ray radiography imaging was initiated 60 s prior to the insertion of the intermediate cell. Images were acquired at a rate of 1 frame/s and continued until the end of the diffusion process. The diffusion axis was set parallel to the direction of gravity, and the zero position of the x-axis was defined at the edge of the alloy sample. The atmospheric pressure was maintained at 5×10^{-2} Pa during the diffusion process. At the end of the diffusion process, each capillary sample was mechanically separated into 20 samples and cooled down to room temperature to solidify.

The samples were weighed and dissolved in a mixture of nitric acid, hydrofluoric acid, and hydrochloric acid in sealed vessels under microwave irradiation (Ethos up, Milestone General). Since Si dissolved in hydrofluoric acid can volatilize as SiF_4, the vessels were allowed to cool completely to room temperature before being opened. To account for volatilization as SiF_4, a standard with a known concentration of Si was dissolved under the same conditions. By comparing the concentration of the standard before and after dissolving the Si sample, the amount of SiF_4 evaporated was quantified, and its ratio was defined as the recovery ratio. The concentrations of Cu and Si in the samples were analyzed by inductively coupled plasma optical emission spectroscopy (ICP-OES; Agilent 5100, Agilent Technologies, Inc.).

4. Results

The intensity profiles along the longitudinal direction of the diffusion couples in Capillaries A and B were obtained from images acquired using XRR. The concentration profiles of Cu were calculated using an intensity-to-concentration conversion formula [16] that adapts the initial Cu concentration to the acquired intensity. Fig. 4 shows the Cu concentration profiles with X-ray images at 973 K obtained from XRR in Capillary A at t = 50, 200, and 700 s. Individual concentration values were calculated using the average intensity of the X-ray image at the corresponding position. Each concentration curve was obtained by fitting the analytical solution of Fick's second law, described as Eq. (1) in Section 2, to the experimental data. During the fitting process, c_0, x_0 and $\langle X^2_{\mathrm{meas}}(t)\rangle_{j\text{-}i}$ were varied as fitting parameters. A concentration profile was obtained for each frame, that is, at each second. The solid lines in Fig. 4 represent the profiles fitted to the analytical model to calculate the MSD at each time step.

The time-resolved MSD of Cu obtained from XRR is referred to as $\langle X^2_{\mathrm{meas}}(t)\rangle_{\mathrm{XRR\_Cu}}$. Fig. 5 shows the time-resolved results of $\langle X^2_{\mathrm{meas}}(t)\rangle_{\mathrm{XRR\_Cu}}$. As described in the analysis model, this measured MSD follows a linear relationship with time. The apparent impurity diffusion coefficient of Cu, $D_{\mathrm{app(Cu)}}$, was determined from the slope of the linear fit, as defined by Eq. (2) in Section 2. The fitting interval was set to 300 s, and the fitting window was shifted by 1 s for each linear fit. As a result, the measured impurity diffusion coefficients of Cu in Capillaries A and B were determined to be $D_{\mathrm{app(Cu)}} = 5.31$ and 5.29×10^{-9} $\mathrm{m^2 s^{-1}}$ at $t = t_{\mathrm{diff}}$, respectively.

Fig. 6 shows the concentration profiles of Cu and Si at 973 K from ICP-OES, respectively. In particular, the Si concentrations were adjusted by applying the recovery ratio determined during dissolution as a correction factor. The recovery ratio averaged 0.991 ± 0.024, and no extreme SiF_4 evaporation was observed. To rigorously account for the uncertainty in the Si recovery ratio, error bars were assigned to the Si concentration profiles. These error bars incorporated both the relative uncertainty of 2.4 % derived from the recovery ratio variation and an absolute uncertainty of 0.1 at % corresponding to the background noise floor determined from the baseline region of the ICP measurements. Similarly, for the Cu concentration profiles, the uncertainty of 0.1 at % derived from the background noise floor was applied as error bars. Fig. 6 indicates that each profile obtained is in good agreement with Eq. (1)

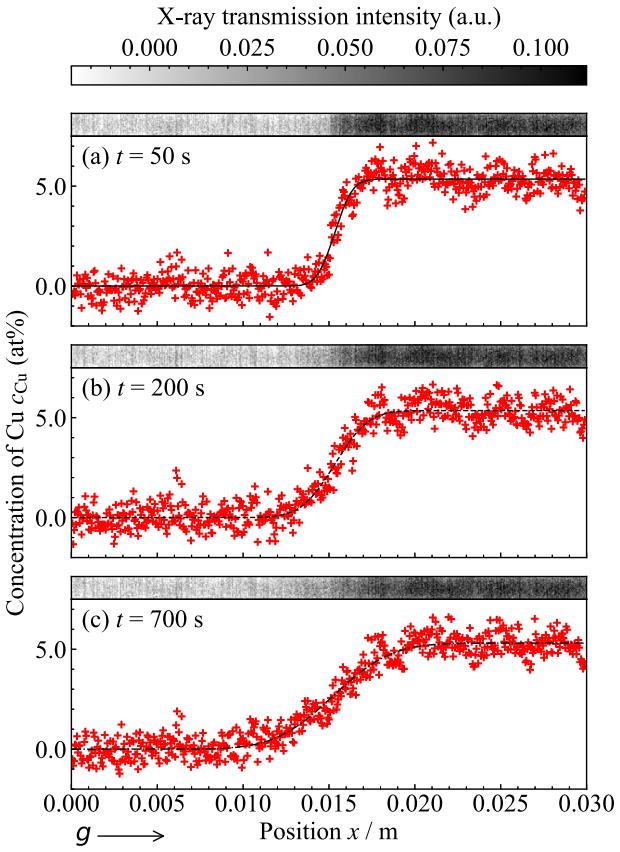

Fig. 4. Measured concentration profiles with X-ray images of Cu obtained by XRR at t of (a) 50 s, (b) 200 s, and (c) 700 s in Capillary A. The corresponding in-situ X-ray images are displayed in the upper panels. Each curve presents the fitting results of X-ray radiography using Eq. (1). The symbol "$g\rightarrow$" indicates the direction of gravity.

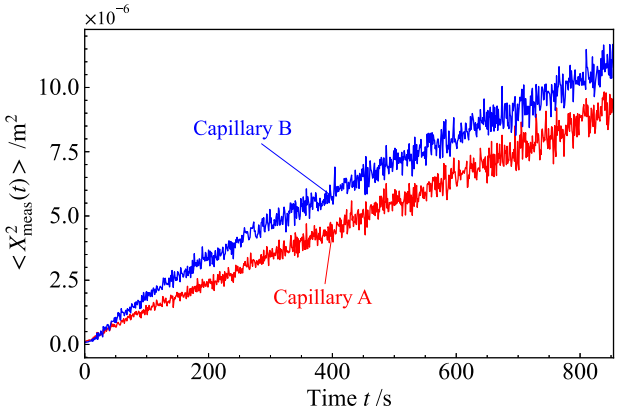

Fig. 5. Time-resolved MSD of Cu obtained by XRR. The red and blue plots present the results in Capillary A and B, respectively.

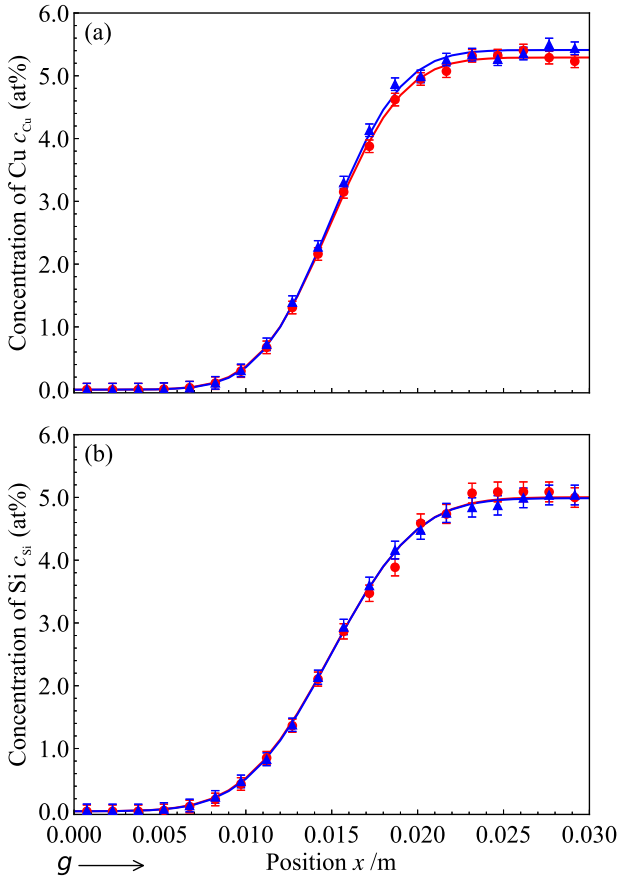

Fig. 6. Measured concentration profiles of (a) Cu and (b) Si at 973 K for two capillaries obtained by ICP-OES. The symbol "$g\rightarrow$" indicates the direction of gravity. The red circle and blue triangle plots present the results in Capillary A and B, respectively. For Cu, the error bars correspond to the background noise floor. The error bars for Si represent the combined uncertainty of the recovery ratio and background noise floor. Each curve presents the fitting results of ICP-OES analysis using Eq. (1).

(coefficient of determination $R^2 > 0.999$): The coefficient of determination R^2 represents the residual between the experimental and fitting values. The value of R^2 closer to 1 indicates a better agreement with the fitting. The MSDs were obtained from the weighted least-squares fitting. Here, the MSDs of Cu and Si from the ICP results are referred to as $\langle X^2_{\mathrm{meas}}(t_{\mathrm{diff}})\rangle_{\mathrm{ICP\_Cu}}$ and $\langle X^2_{\mathrm{meas}}(t_{\mathrm{diff}})\rangle_{\mathrm{ICP\_Si}}$, respectively. The values of $\langle X^2_{\mathrm{meas}}(t_{\mathrm{diff}})\rangle_{\mathrm{ICP\_Cu}}$ for Capillaries A and B were (1.12 ± 0.08) and (1.08 ± 0.08) × 10^{-5} m^2, respectively. The values of $\langle X^2_{\mathrm{meas}}(t_{\mathrm{diff}})\rangle_{\mathrm{ICP\_Si}}$ for Capillaries A and B were (1.57 ± 0.13) and (1.53 ± 0.12) × 10^{-5} m^2, respectively. Here, the uncertainties represent the standard error derived from the weighted fitting process.

5. Discussion

First, the suppression of natural convection during the diffusion experiment is demonstrated based on the impurity diffusion coefficient of Cu obtained from the results. Subsequently, the shear convection that occurred during the experiment is quantitatively evaluated using the MSDs derived from both XRR and ICP measurements of Cu. Based on the quantified shear convection, the impurity diffusion coefficient of Si in liquid Al is then determined.

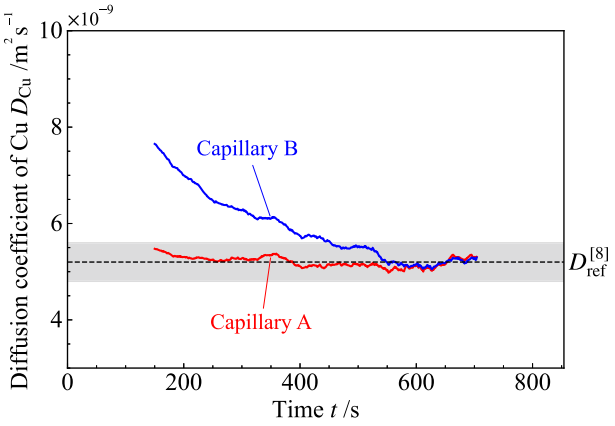

Fig. 7. Apparent impurity diffusion coefficients of Cu in liquid Al at 973 K. The red and blue plots present the D_{Cu} in Capillaries A and B, respectively. The dashed line and gray area represent the reference data [11] and its uncertainty, respectively.

5.1. Investigation of suppressing natural convection in the diffusion experiments

Fig. 7 shows the apparent impurity diffusion coefficients of Cu obtained in the experiment, along with the value reported in a previous study [11] where natural convection was confirmed to be suppressed. The apparent diffusion coefficient represents the average over the fitting interval for the linear fit, and the midpoint of that interval was plotted as the corresponding time for the apparent diffusion coefficient. Since the results of the previous study were obtained using the identical XRR apparatus and the same analysis method, systematic errors arising from the equipment or analysis procedure are considered negligible. For Capillary A, the measured values fluctuated consistently within the error bars of the previous study throughout the entire duration. In contrast, Capillary B exhibited a pronounced influence of shear convection caused by the insertion of the intermediate cell at the initial stage; however, the values gradually converged within the error range of the previous study as time progressed. This initial effect was also evident from the time-resolved increase in $\langle X^2_{\mathrm{meas}}(t)\rangle_{\mathrm{XRR\_Cu}}$ shown in Fig. 5. These results indicate that this diffusion experiment was conducted under conditions where natural convection was suppressed. In addition, the impurity diffusion coefficient of Cu was measured in an alloy containing both Cu and Si. However, these values agree within the error bars with those previously reported for Al–Cu alloys containing only Cu [11]. Therefore, the influence of Si on the impurity diffusion coefficient of Cu is considered negligible.

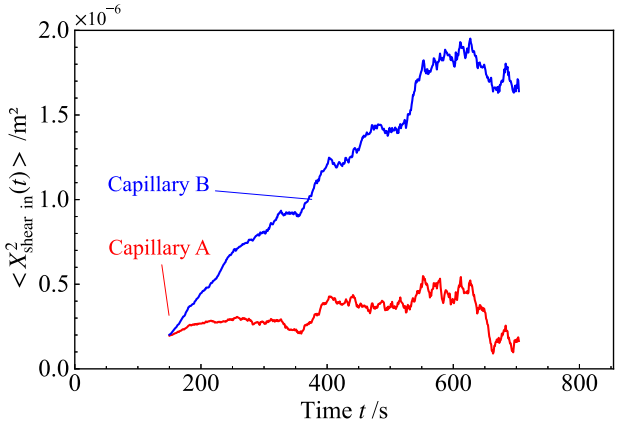

Fig. 8. Time-evolved MSD of Cu representing the shear convection by the insertion of the intermediate cell.

5.2. Correction methodology of the shear convection in the diffusion experiments

Fig. 8 shows the interceptions, $\langle X^2_{\text{shear in}} \rangle$, derived from applying Eq. (2) to Fig. 5. The fitting interval was set to 300 s, and the fitting window was shifted by 1 s for each linear fit. The midpoint of that interval was plotted as the corresponding time for the interception. Although $\langle X^2_{\text{shear in}} \rangle$ is theoretically expected to be a constant value in Fig. 2, Fig. 8 reveals that it evolves over time. This behavior, particularly the pronounced variation in Capillary B, can be explained by a combination of a physical damping process and a mathematical artifact from our analysis method. Physically, the shear convection generated instantaneously upon cell insertion is not a persistent flow. As demonstrated by the model experiments and simulations of Griesche et al. [14], the initial high-velocity convection roll is damped significantly by the viscosity, decaying rapidly after the shear movement stops. This physical damping process is clearly observed in our own experiment in Fig. 7. The apparent diffusion coefficient $D_{\text{app(Cu)}}$, which includes the convective contribution, is initially high and monotonically decreases over time, stabilizing at the true diffusive value (D_{ref}) after approximately 600 s. This indicates that the initial shear convection in our system takes about 600 s to completely dissipate. The $\langle X^2_{\text{shear in}} \rangle$ plotted in Fig. 8 is not a direct physical measurement, but rather the y-intercept derived from a 300-second moving linear fit applied to the MSD data (Fig. 5). For $t <$ 600 s, the fitting window is operating on data from the "convective-decay regime" (Fig. 7), where the MSD slope is continuously decreasing (i.e., the data is non-linear). Applying a linear fit to this non-linear, concave-down curve will mathematically cause the extrapolated y-intercept to be distorted and appear to increase. The peak near 600 s corresponds to the fitting window transitioning from this non-linear "damping" regime into the stable, purely diffusive (and thus truly linear) regime. The subsequent "decrease" in Fig. 8 (for $t >$ 600 s) is the mathematical artifact of the fit "settling" onto the true, stable intercept value, as the fitting window now operates entirely within the stable, linear diffusive data.

In contrast to this behavior in Capillary B, Capillary A exhibited a relatively small influence from shear convection during cell insertion. This is strongly supported by Fig. 7, which shows that the $D_{\text{app(Cu)}}$ for Capillary A was stable and consistent with the reference value [11] almost immediately from the start of the experiment. Consequently, the MSD data for Capillary A (Fig. 5) is considered to have been in a linear, diffusion-dominated regime from an early stage. Therefore, the mathematical artifact seen in Capillary B is presumed to be minimal in Capillary A. The behavior observed for Capillary A in Fig. 8 (a low overall value and minor fluctuations of $\langle X^2_{\text{shear in}} \rangle$) is thus not interpreted as reflecting a significant physical damping process. Instead, it is considered to primarily reflect the statistical fitting errors and uncertainties inherent in applying a moving linear fit to MSD data that contains intrinsic XRR noise.

Furthermore, a notable feature in Fig. 8 is that the minor fluctuations in $\langle X^2_{\text{shear in}} \rangle$ appear to be partially correlated between Capillaries A and B (e.g., the similar increasing/decreasing trends around 400–600 s). This suggests the presence of a systematic experimental artifact that affected both samples simultaneously. One probable cause is minor fluctuations in the X-ray source intensity or detector sensitivity. Such changes would simultaneously affect the concentration calculations for both samples, introducing correlated noise into the MSD values. This noise would then propagate through the intercept calculation, appearing as the correlated fluctuations observed in Fig. 8.

Fig. 9 presents a comparison of $\langle X^2_{\text{shear in}} \rangle$, the MSD at the end of the diffusion process $\langle X^2_{\text{meas}}(t_{\text{diff}}) \rangle_{\text{XRR\_Cu}}$, and the MSD obtained from ICP-OES $\langle X^2_{\text{meas}}(t_{\text{diff}}) \rangle_{\text{ICP\_Cu}}$. A straight line represents the linear fit to 300 s, including the end of the diffusion process, and the intercept corresponds to $\langle X^2_{\text{shear in}} \rangle$. In Capillary A, shown in Fig. 9(a), the influence of

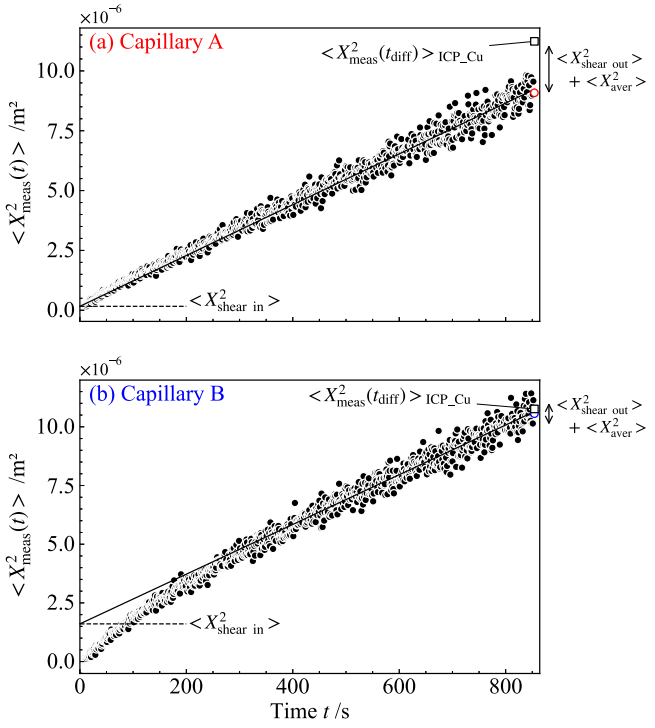

Fig. 9. Time-resolved MSD of Cu with $\langle X^2_{\text{shear in}} \rangle$, $\langle X^2_{\text{shear out}} \rangle$, $\langle X^2_{\text{aver}} \rangle$, and $\langle X^2_{\text{meas}}(t_{\text{diff}}) \rangle_{\text{ICP\_Cu}}$: (a) Capillary A, and (b) Capillary B. The linear fit over a 300 s interval, including the end of the diffusion process, is represented by a straight line. The y-intercept of the line represents $\langle X^2_{\text{shear in}} \rangle$. The black plots are the same in Fig. 5. Especially, the open red and blue circles indicate the MSDs at the end of the diffusion process for Capillaries A and B, respectively. The open square presents $\langle X^2_{\text{meas}}(t_{\text{diff}}) \rangle_{\text{ICP\_Cu}}$. The value obtained by subtracting the open square from $\langle X^2_{\text{meas}}(t_{\text{diff}}) \rangle_{\text{XRR\_Cu}}$ represents the amount of $\langle X^2_{\text{shear out}} \rangle$ and $\langle X^2_{\text{aver}} \rangle$.

shear convection during cell insertion was relatively small, while that during cell separation was significant. In contrast, Capillary B, shown in Fig. 9(b), exhibited remarkable shear convection during cell insertion but a negligible influence during separation. Here, the MSD obtained by subtracting $\langle X^2_{\text{meas}}(t_{\text{diff}}) \rangle_{\text{XRR\_Cu}}$ at the end of diffusion process from $\langle X^2_{\text{meas}}(t_{\text{diff}}) \rangle_{\text{ICP\_Cu}}$ is defined as $\langle X^2_{\text{shear out}} \rangle + \langle X^2_{\text{aver}} \rangle$. Therefore, the shear convection can be quantitatively expressed during the diffusion experiment. Table 1 summarizes the values of $\langle X^2_{\text{shear in}}(t_{\text{diff}}) \rangle$ and $\langle X^2_{\text{shear out}} \rangle + \langle X^2_{\text{aver}} \rangle$ for each capillary. To evaluate the reliability of these experimental values, their associated standard uncertainties are also presented in Table 1. The uncertainty for $\langle X^2_{\text{shear in}}(t_{\text{diff}}) \rangle$ corresponds to the standard error of the intercept derived from the time-resolved XRR analysis. Crucially, the value of $\langle X^2_{\text{shear out}} \rangle + \langle X^2_{\text{aver}} \rangle$ is determined by subtracting the MSD measured by XRR at the end of the diffusion process from the MSD obtained by ICP-OES. Therefore, its uncertainty was calculated using the law of propagation of error, synthesizing both the fitting uncertainty of $\langle X^2_{\text{meas}}(t_{\text{diff}}) \rangle_{\text{ICP\_Cu}}$ and the regression uncertainty of the XRR data. The latter was evaluated to be

Table 1
Summary of $\langle X^2_{\text{shear in}}(t_{\text{diff}}) \rangle$ and $\langle X^2_{\text{shear out}} \rangle + \langle X^2_{\text{aver}} \rangle$ with their associated uncertainties for Capillaries A and B.

Label	$\langle X^2_{\text{shear in}}(t_{\text{diff}}) \rangle$ (m²)	$\langle X^2_{\text{shear out}} \rangle + \langle X^2_{\text{aver}} \rangle$ (m²)
Capillary A	$(0.16 \pm 0.18) \times 10^{-6}$	$(2.15 \pm 0.91) \times 10^{-6}$
Capillary B	$(1.61 \pm 0.17) \times 10^{-6}$	$(0.20 \pm 0.86) \times 10^{-6}$

Note: Standard uncertainty is indicated by the value following the ± symbol.

4.0 and 3.8 × 10^{-7} m^2 for Capillaries A and B, respectively, based on the residual analysis of the time-resolved MSD at the end of the diffusion process. This quantitative breakdown highlights that the precision of the correction depends on the combined accuracy of both measurement techniques.

As shown in Table 1 and Fig. 9, the relative contributions of shear convection during insertion $\langle X^2_{\text{shear in}}(t_{\text{diff}})\rangle$ and $\langle X^2_{\text{shear out}}\rangle + \langle X^2_{\text{aver}}\rangle$ differ significantly between Capillaries A and B. This discrepancy is likely attributed to slight, unavoidable misalignments or variations in the mechanical operation during the shear processes. It is important to note that, despite these large variations in the measured convective components, this correction methodology allows for the effective isolation of these arbitrary mechanical effects. As will be shown in the following section, applying this correction yields consistent results for the purely diffusive component of Si. This demonstrates the robustness of our combined XRR and shear cell approach in determining the true diffusion coefficient, even in the presence of varied experimental artifacts.

The applicability of this methodology to other temperatures is maintained by the in-situ calibration using the Cu tracer. Therefore, no additional theoretical corrections are required for temperature changes. However, experimental parameters require adjustment at higher temperatures. The diffusion time must be reduced to satisfy the semi-infinite boundary condition due to faster diffusion. Furthermore, reduced viscosity may prolong the damping time of shear convection. The convection might not reach a stable state within a limited diffusion time. Consequently, rigorous verification against the reference diffusion coefficient of the tracer is essential. This process ensures the accurate evaluation of the impact of additional mass transport.

5.3. Impurity diffusion coefficient of Si in liquid Al corrected for the additional mass transport induced by shear convection

Finally, considering the discussion above, the impurity diffusion coefficient of Si in liquid Al is calculated. Two corrections are applied to the MSD obtained from the concentration profiles of Si from ICP-OES: one for the shear convection quantified in the previous section, and one for the averaging effect defined as $\langle X^2_{\text{aver}}\rangle$ arising from subdividing the sample prior to ICP analysis [8]. The value of $\langle X^2_{\text{aver}}\rangle$ is obtained from the plot of the average concentration value for each cell. This effect can be described geometrically as $H^2/12$ ($\langle X^2_{\text{aver}}\rangle = H^2/12 = 1.9 \times 10^{-7}$ m^2, where $H = 1.5 \times 10^{-3}$ m) [8]. To account for the uncertainty arising from the segmentation process, a machining tolerance of $H \pm 0.1 \times 10^{-3}$ m was considered. The resulting uncertainty was estimated to be approximately 0.3 × 10^{-7} m^2. Accordingly, the impurity diffusion coefficient of Si in liquid Al D_{Si} is determined from the following equation.

$$D_{\text{Si}} = \frac{\langle X^2_{\text{meas}}(t_{\text{diff}})\rangle_{\text{ICP\_Si}} - \langle X^2_{\text{shear in}}(t_{\text{diff}})\rangle - (\langle X^2_{\text{shear out}}\rangle + \langle X^2_{\text{aver}}\rangle)}{2t_{\text{diff}}}. \quad (3)$$

In addition, the uncertainty of D_{Si} was derived to evaluate the experimental precision. To quantify the reliability of the obtained values, four uncertainty components corresponding to the MSD terms were defined. Specifically, $U_{\text{ICP\_Si}}$ and $U_{\text{shear in}}(t_{\text{diff}})$ represent the uncertainties for $\langle X^2_{\text{meas}}(t_{\text{diff}})\rangle_{\text{ICP\_Si}}$ and $\langle X^2_{\text{shear in}}(t_{\text{diff}})\rangle$, respectively. Regarding the other corrections, $U_{\text{shear out + aver}}$ denotes the uncertainty of the experimental value $\langle X^2_{\text{shear out}}\rangle + \langle X^2_{\text{aver}}\rangle$ determined by the Cu tracer, whereas U_{aver} represents the uncertainty of the geometric factor $\langle X^2_{\text{aver}}\rangle$ itself. Consequently, the total uncertainty of D_{Si}, denoted as $U(D_{\text{Si}})$, was calculated based on the error propagation law as expressed in Eq. (4):

$$U(D_{\text{Si}}) = \frac{1}{2t_{\text{diff}}}\sqrt{U^2_{\text{ICP\_Si}} + U^2_{\text{shear in}}(t_{\text{diff}}) + U^2_{\text{shear out + aver}} + U^2_{\text{aver}}}. \quad (4)$$

From Eqs. (3) and (4), the measured impurity diffusion coefficients of Si in liquid Al were found to be (7.78 ± 0.91) and (7.84 ± 0.88) × 10^{-9} m^2s^{-1} for Capillaries A and B, respectively. Remarkably, these values exhibit agreement despite the significant difference in shear convection observed between the two samples. This consistency demonstrates the robustness of the present methodology in isolating and subtracting convective contributions. Consequently, the average value of (7.81 ± 0.90) × 10^{-9} m^2s^{-1} is adopted as the reliable impurity diffusion coefficient of Si.

Furthermore, the value at 973 K extrapolated using the Arrhenius law reported by Kikuchi et al. in a previous study [10] was (9.7 ± 0.8) × 10^{-9} m^2s^{-1}, whereas the present results are lower. This discrepancy arises because the previous measurement was conducted using the capillary reservoir method, in which mechanical convection during the experiment likely led to an overestimation of D_{Si}.

5.4. Effect of thermodynamic coupling in the Al-Cu-Si system on the impurity diffusion coefficient of Si

In this study, the impurity diffusion coefficient of Si is determined by subtracting the shear convection, quantified from the XRR data for Cu, from the apparent MSD of Si obtained from ICP-OES analysis. This approach is predicated on using Cu as a "tracer," which introduces a significant challenge: our experiment is a ternary (Al-Cu-Si) system, not the binary (Al-Si) system of interest. Therefore, it is imperative to ascertain that the presence and strong concentration gradient of the Cu tracer do not thermodynamically interfere with the diffusional flux of Si.

In a multicomponent system, the diffusional flux of one component is driven not only by its own concentration gradient but also by the gradients of all other components, as described by Onsager relations [17,18]. In the Fick's law formalism, this relationship is captured by the diffusion coefficient matrix [D]. This diffusion matrix can be expressed as the product of a mobility matrix [M], which represents the kinetic contribution and is derived from the fundamental Onsager coefficients, and a matrix of the thermodynamic factor [Γ] (i.e., [D] = [M][Γ]). The thermodynamic factor matrix quantifies the thermodynamic driving forces for diffusion. The diagonal terms (e.g., Γ_{SiSi}) represent the main driving force, while the off-diagonal terms (e.g., Γ_{SiCu}) quantify the thermodynamic coupling; that is, how the flux of Si is influenced by the concentration gradient of Cu. If this Γ_{SiCu} term is negligibly small compared to the diagonal Γ_{SiSi} term, it implies that the diffusional interaction (coupling) is minimal. This would validate our assumption that the presence of the Cu tracer does not significantly distort the measurement of Si diffusion. Therefore, to directly evaluate this coupling in our system, we calculated the thermodynamic factors.

To further validate this assumption directly for the Al-Cu-Si system, the thermodynamic factors denoted as $\Gamma_{\alpha\beta}$ at 973 K were calculated. The components α and β refer to the impurity elements, Cu and Si. In a ternary system the matrix of thermodynamic factors [$\Gamma_{\alpha\beta}$] is related to the Hessian matrix [$H_{\alpha\beta}$], which contains the second partial derivatives of the molar Gibbs free energy G_{m}. The Hessian matrix is defined as:

$$H_{\alpha\beta} = \frac{1}{RT}\left(\frac{\partial^2 G_{\text{m}}}{\partial N_\alpha \partial N_\beta}\right). \quad (5)$$

Here R is gas constant, T is temperature, and N is molar fraction of the element indicated by subscript. The relationship between the [$\Gamma_{\alpha\beta}$] and [$H_{\alpha\beta}$] matrices is given by[17]

$$\begin{bmatrix}\Gamma_{\text{CuCu}} & \Gamma_{\text{CuSi}}\\ \Gamma_{\text{SiCu}} & \Gamma_{\text{SiSi}}\end{bmatrix} = \begin{bmatrix}(1-N_{\text{Cu}})N_{\text{Cu}} & -N_{\text{Cu}}N_{\text{Si}}\\ -N_{\text{Cu}}N_{\text{Si}} & (1-N_{\text{Si}})N_{\text{Si}}\end{bmatrix}\begin{bmatrix}H_{\text{CuCu}} & H_{\text{CuSi}}\\ H_{\text{SiCu}} & H_{\text{SiSi}}\end{bmatrix}. \quad (6)$$

The [$H_{\alpha\beta}$] was then computed by numerically differentiating the G_{m} data which can be described by the Redlich-Kister polynomial coefficients [19,20]. The detailed calculation method is shown in Appendix A. Finally, the thermodynamic factors $\Gamma_{\alpha\beta}$ were determined using the

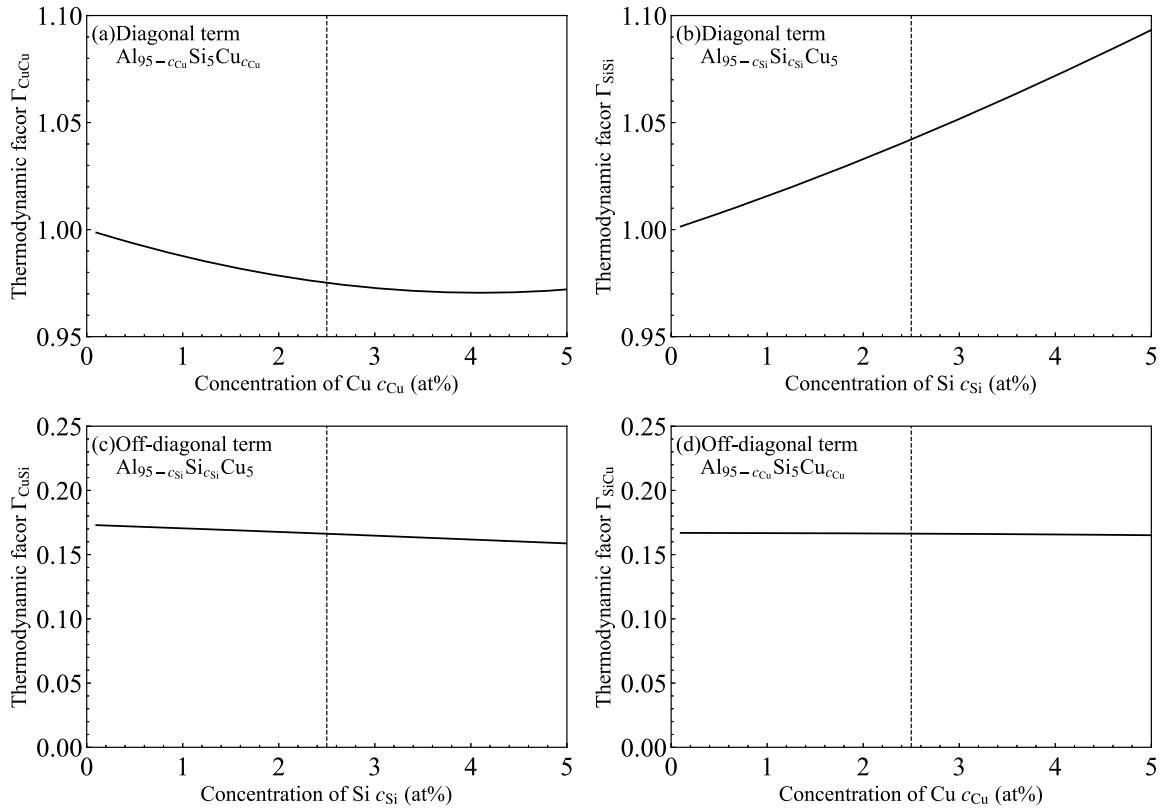

Fig. 10. Calculated thermodynamic factors in the liquid Al-Cu-Si system at 973 K. (a) Diagonal term Γ_{CuCu} as a function of Cu concentration with the Si concentration fixed at 5 at %. (b) Diagonal term Γ_{SiSi} as a function of Si concentration with the Cu concentration fixed at 5 at %. (c) Off-diagonal term Γ_{CuSi} as a function of Si concentration with the Cu concentration fixed at 5 at %. (d) Off-diagonal term Γ_{SiCu} as a function of Cu concentration with the Si concentration fixed at 5 at %. The vertical dashed lines indicate the approximate average concentration (2.5 at %) of the diffusion couple.

equation above with a custom-developed numerical code.

The results of this calculation are shown in Fig. 10. Fig. 10(a) and (b) show the diagonal thermodynamic factors, which represent the main driving forces for the diffusion of Cu and Si, respectively. Their values at the approximate average concentration of the diffusion couple are $\Gamma_{CuCu} \approx 0.97$ and $\Gamma_{SiSi} \approx 1.05$ with c_{Cu} and c_{Si} at 2.5 at %, respectively. Fig. 10(c) and (d) show the off-diagonal factors, Γ_{CuSi} and Γ_{SiCu}, which represent the thermodynamic coupling between the Cu flux and the Si concentration gradient, and between the Si flux and the Cu concentration gradient, respectively. Both Γ_{CuSi} and Γ_{SiCu} show a near-constant value of approximately 0.17 across the relevant concentration range. This calculated interaction (0.17) is approximately 6 times smaller than the main diagonal driving forces (0.97 and 1.05).

This finding of small thermodynamic coupling is consistent with experimental work in similar aluminum-based ternary alloys. For instance, Engelhardt et al. conducted a detailed analysis of diffusion in the liquid Al-Ag-Cu eutectic alloy and demonstrated experimentally that the off-diagonal terms (cross-terms) of the diffusion matrix are several orders of magnitude smaller than the diagonal terms [21]. Crucially, we can validate the actual impact of this calculated interaction term. The term Γ_{CuSi} (Fig. 10(c)) represents the thermodynamic effect of the Si gradient on the Cu flux. In Section 5.1, we experimentally observed that the diffusion of Cu was not affected by the presence of Si. This proves that the calculated thermodynamic interaction of 0.17 with c_{Si} at 2.5 at % is experimentally negligible and its effect is fully contained within the uncertainty of the measurement. Given this, we can now assess the term Γ_{SiCu} (Fig. 10(d)), which is the primary concern for our correction methodology (the effect of Cu on Si). Since this calculated value ($\approx$0.17) is identical in magnitude to the Γ_{CuSi} term just proven to be experimentally negligible, it is reasonable to conclude that the influence of the Cu gradient on Si diffusion is also minimal and well within the overall experimental uncertainty. Therefore, the application of the mechanical convection effect, as measured using Cu as a tracer, to the diffusion of Si represents a valid approximation for determining the precise impurity diffusion coefficient of Si.

The validation in the Al-Cu-Si system generalizes the applicability of this methodology. Specifically, three criteria must be satisfied for the extension of this methodology to other systems. First, the tracer must possess a sufficiently different X-ray absorption coefficient compared to the other components to ensure high contrast. Second, as demonstrated above, the thermodynamic cross-coupling effect must be negligible. Significant coupling would invalidate the use of the tracer for the target element. Third, the system must inherently support stable density layering. This requires a monotonic density change with concentration to ensure hydrodynamic stability against natural convection. Regarding the stability of the alloy system, Suzuki et al. [22] have summarized the applicability of the shear cell technique, which serves as a useful reference.

6. Conclusions

The impurity diffusion coefficients of Si in liquid Al alloys at 973 K were measured using the combined XRR and shear cell technique. Adding Cu to the Al-Si system enabled stable density layering. The in-situ XRR observation of Cu concentration profiles confirmed that natural convection was effectively suppressed during the diffusion process. Crucially, this study demonstrated the feasibility of quantifying and correcting for additional mass transport induced by shear convection. This correction was achieved by quantitatively isolating the mechanical mass transports, using Cu as a tracer. The initial mass transport from cell insertion was derived from the intercept of in-situ XRR data. Subsequently, the final mass transport from cell separation was determined by

the difference between the final XRR and ICP results. Consequently, the impurity diffusion coefficient of Si was determined to be (7.81 ± 0.90) × 10^{-9} m^2s^{-1} at 973 K. The validity of applying this Cu tracer to Si was further supported by a supplementary analysis of the thermodynamic factors, which demonstrated that the diffusional coupling between Cu and Si in the liquid Al-Cu-Si system is negligible.

However, the application of this methodology requires careful attention to the X-ray absorption of the tracer, thermodynamic interactions with the solute, and the stability of density layering. Provided these criteria are satisfied, the methodology is applicable to a wide range of metallic systems beyond ternary alloys, where components other than the tracer are X-ray transparent.

CRediT authorship contribution statement

Masato Shiinoki: Writing – review & editing, Writing – original draft, Visualization, Validation, Software, Methodology, Investigation, Funding acquisition, Formal analysis, Data curation, Conceptualization. **Elke Sondermann:** Writing – review & editing, Formal analysis, Data curation. **Andreas Meyer:** Writing – review & editing, Supervision, Project administration, Funding acquisition, Formal analysis, Data curation, Conceptualization. **Shinsuke Suzuki:** Writing – review & editing, Supervision, Project administration, Funding acquisition, Formal analysis, Data curation, Conceptualization.

Declaration of competing interest

The authors declare that they have no known competing financial interests or personal relationships that could have appeared to influence the work reported in this paper.

Acknowledgements

This study was supported by Grant-in-Aid for Scientific Research(C) Grant Number JP23K04364, Grant-in-Aid for Research Activity Start-up Grant Number JP24K23035, Grant-in-Aid for Early-Career Scientists Grant Number JP25K17819, German Aerospace Center and the German Academic Exchange Service (DLR/DAAD) Research Fellowships (No. 57622550), Light Metal Educational Foundation for founding (Project number: 2025-B-128) and Waseda University Grant for Special Research Projects (Project number: 2024C-709 and 2025C-419). We thank Kimura Foundry Co., Ltd. for financial support and Kagami Memorial Research Institute for Materials Science and Technology for technical support.

Appendix A: Thermodynamic model for the Al-Cu-Si system

The molar Gibbs free energy G_m of the liquid Al-Cu-Si ternary system was described using the Redlich-Kister polynomial expansion. The total molar Gibbs free energy of the system is expressed as:

$$G_m = G_{ref} + G_{ideal} + G_{ex}. \tag{A1}$$

Here G_{ref} is the reference Gibbs free energy of the pure components, G_{ideal} is the ideal mixing Gibbs free energy, and G_{ex} is the excess Gibbs free energy.

$$G_{ideal} = RT(N_{Al}\ln(N_{Al}) + N_{Cu}\ln(N_{Cu}) + N_{Si}\ln(N_{Si})). \tag{A2}$$

The G_{ex} is the sum of the binary and the ternary contributions.

$$G_{ex} = N_{Al}N_{Cu}L_{Al,Cu} + N_{Al}N_{Si}L_{Al,Si} + N_{Cu}N_{Si}L_{Cu,Si} + N_{Al}N_{Cu}N_{Si}L_{Al,Cu,Si}. \tag{A3}$$

Each binary interaction parameter L_{mn} is expanded as a function of composition:

$$L_{mn} = \sum_{l=0}^{s} {}^{(l)}L_{mn}(N_m - N_n)^l, \tag{A4}$$

Here ${}^{(l)}L_{mn}$ are the l-th order binary interaction parameters, which are temperature-dependent. The ternary interaction parameter $L_{Al,Cu,Si}$ can also be expanded, although it is often simplified in liquid systems.

$$L_{Al,Cu,Si} = N_{Al}L^{Al}_{Al,Cu,Si} + N_{Cu}L^{Cu}_{Al,Cu,Si} + N_{Si}L^{Si}_{Al,Cu,Si}. \tag{A5}$$

Tables A1 and A2 show the summary of binary and ternary interaction parameters for the liquid Al-Cu-Si system, respectively. The thermodynamic factors [Γ] presented in Section 5.4 were derived by numerically calculating the second partial derivatives of the G_m using Eq. (5). It should be noted that the G_{ref} term in Eq. (A1) is independent of the molar fractions. Consequently, its second partial derivatives with respect to concentration are zero, and thus G_{ref} does not contribute to the calculation of the Hessian matrix. Only the G_{ideal} and G_{ex} determine the thermodynamic factors.

Table A1
Summary of binary interaction parameters for the liquid Al-Cu-Si system.

Model (*m*, *n*)	Interaction parameter (J/mol)	Reference
(Al, Cu)	${}^{(0)}L_{Al,Cu} = -67094 + 8.555T$	[23]
	${}^{(1)}L_{Al,Cu} = 32148 + 7.118T$	
	${}^{(2)}L_{Al,Cu} = 5915 - 5.889T$	
	${}^{(3)}L_{Al,Cu} = -7290 + 5.5T$	
(Al, Si)	${}^{(0)}L_{Al,Si} = -11340.1 - 1.23394T$	[24]
	${}^{(1)}L_{Al,Si} = -3530.93 + 1.35993T$	

(*continued on next page*)

Table A1 (*continued*)

Model (*m*, *n*)	Interaction parameter (J/mol)	Reference
(Cu, Si)	${}^{(2)}L_{Al,Si} = 2265.39$ ${}^{(0)}L_{Cu,Si} = -37776 + 3.47T$ ${}^{(1)}L_{Cu,Si} = -44866 + 14.53T$ ${}^{(2)}L_{Cu,Si} = -40866 + 8.62T$ ${}^{(3)}L_{Cu,Si} = -10060$ ${}^{(4)}L_{Cu,Si} = 17550$	[25]

T: Temperature.

Table A2
Summary of ternary interaction parameters for the liquid Al-Cu-Si system.

Model	Interaction parameter (J/mol)	Reference
(Al, Cu, Si)	$L^{Al}_{Al,Cu,Si} = 40000$ $L^{Cu}_{Al,Cu,Si} = 50000$ $L^{Si}_{Al,Cu,Si} = -10000$	[25]

Data availability

Data will be made available on request.

References

[1] A. Noeppel, A. Ciobanas, X.D. Wang, K. Zaidat, N. Mangelinck, O. Budenkova, A. Weiss, G. Zimmermann, Y. Fautrelle, Influence of forced/natural convection on segregation during the directional solidification of Al-based binary alloys, Metall. Mater. Trans. B 41 (2010) 193–208, https://doi.org/10.1007/s11663-009-9311-6.

[2] Y. Ai, Y. Zhang, S. Han, X. Liu, Numerical investigation on the molten pool and keyhole dynamic behaviors and weld microstructure in laser-induction hybrid welding of stainless steel, Int. J. Heat Mass Transf. 245 (2025) 126988, https://doi.org/10.1016/j.ijheatmasstransfer.2025.126988.

[3] T. Schiller, E. Sondermann, A. Meyer, New analyzing approaches for in situ interdiffusion experiments to determine concentration-dependent diffusion coefficients in liquid Al–Au, Metals 11 (2021) 1772, https://doi.org/10.3390/met11111772.

[4] M. Uhida, Y. Watanabe, S. Matsumoto, M. Kaneko, T. Fukazawa, T. Masaki, T. Itami, X-ray observation of shear cell experiments for impurity diffusion of Au in liquid Ag, J. Non Cryst. Solids 312–314 (2002) 203–207, https://doi.org/10.1016/s0022-3093(02)01697-6.

[5] C. Neumann, E. Sondermann, F. Kargl, A. Meyer, Compact high-temperature shear-cell furnace for in-situ diffusion measurements, J. Phys. Conf. Ser. 327 (2011) 012052, https://doi.org/10.1088/1742-6596/327/1/012052.

[6] Y. Kobayashi, M. Shiinoki, T. Masaki, S. Suzuki, Measurements of diffusion coefficients in liquid alloys using two measurement points of in situ X-ray fluorescence analysis, Defect Diffus. Forum 439 (2025) 127–138, https://doi.org/10.4028/p-mi3qpt.

[7] T. Ujihara, K. Fujiwara, G. Sazaki, N. Usami, K. Nakajima, Simultaneous in situ measurement of solute and temperature distributions in the alloy solutions, J. Cryst. Growth 242 (2002) 313–320, https://doi.org/10.1016/s0022-0248(02)01423-9.

[8] S. Suzuki, K.-H. Kraatz, G. Frohberg, Ground-based diffusion experiments on liquid Sn-In systems using the shear cell technique of the satellite mission Foton-M1, Ann. N. Y. Acad. Sci. 1027 (2004) 169–181, https://doi.org/10.1196/annals.1324.016.

[9] L. Zhong, J. Hu, Y. Geng, C. Zhu, B. Zhang, A multi-slice sliding cell technique for diffusion measurements in liquid metals, Rev. Sci. Instrum. 88 (2017) 093905, https://doi.org/10.1063/1.5003623.

[10] T. Kikuchi, K. Tani, Diffusion of silicon, iron and copper in molten aluminum, Niihama National College of Technology Bulletin 30 (1994) 34–37.

[11] E. Sondermann, N. Jakse, K. Binder, A. Mielke, D. Heuskin, F. Kargl, A. Meyer, Concentration dependence of interdiffusion in aluminum-rich Al-Cu melts, Phys. Rev. B Condens. Matter 99 (2019) 024204, https://doi.org/10.1103/PhysRevB.99.024204.

[12] S. Suzuki, K.-H. Kraatz, G. Frohberg, Reduction of convection in diffusion measurement using the shear cell by stabilization of density layering on the ground, J. Jpn. Soc. Microgravity Appl. 28 (2011) 100, https://doi.org/10.15011/jasma.28.2.100.

[13] M. Shiinoki, Y. Nishimura, K. Noboribayashi, S. Suzuki, Suppressing natural convection for self-diffusion measurement in liquid Pb using shear cell technique by stable density layering of isotopic concentration, Metall. Mater. Trans. B 52 (2021) 3846–3859, https://doi.org/10.1007/s11663-021-02300-9.

[14] A. Griesche, K.-H. Kraatz, G. Frohberg, G. Mathiak, R. Willnecker, Liquid diffusion measurements with the shear cell technique - study of shear convection, microgravity research and aplications in physical sciences and biotechnology, in: Proceedings of the First International Symposium Held 10-15 September, 2001, 2000 in Sorrento, Italy. Edited by O. Minster and B. Schürmann.

[15] J.L. Hu, P. Wang, Y.H. Jia, Z.C. Fang, F.Q. Huang, J. Guo, B. Zhang, A liquid metal diffusion measurement technique integrating the x-ray radiography and multi-slice sliding cell, Rev. Sci. Instrum. 95 (2024), https://doi.org/10.1063/5.0213417.

[16] A. Griesche, B. Zhang, E. Solórzano, F. Garcia-Moreno, Note: x-ray radiography for measuring chemical diffusion in metallic melts, Rev. Sci. Instrum. 81 (2010) 056104, https://doi.org/10.1063/1.3427256.

[17] R. Taylor, R. Krishna, Multicomponent Mass Transfer, John Wiley & Sons, Nashville, TN, 1993.

[18] L. Onsager, Theories and problems of liquid diffusion, Ann. N. Y. Acad. Sci. 46 (1945) 241–265, https://doi.org/10.1111/j.1749-6632.1945.tb36170.x.

[19] O. Redlich, A.T. Kister, Algebraic representation of thermodynamic properties and the classification of solutions, Ind. Eng. Chem. 40 (1948) 345–348, https://doi.org/10.1021/ie50458a036.

[20] H. Lukas, S.G. Fries, B. Sundman, Computational Thermodynamics: The Calphad Method, Cambridge University Press, Cambridge, England, 2007.

[21] M. Engelhardt, F. Kargl, E. Sondermann, A. Meyer, Kinetic contributions rule diffusion of mass in the liquid ternary eutectic E1 Ag-Al-Cu alloy, J. Phys. Condens. Matter 37 (2025), https://doi.org/10.1088/1361-648X/ae0259.

[22] S. Suzuki, K.-H. Kraatz, G. Frohberg, Diffusion experiments in liquid Sn-Bi and Al-Ni systems with a stable density layering using the FOTON shear cell under 1g conditions, Microgravity Sci. Technol. 16 (2005) 120–126, https://doi.org/10.1007/BF02945961.

[23] S.-M. Liang, R. Schmid-Fetzer, Thermodynamic assessment of the Al–Cu–Zn system, part II: al–Cu binary system, CALPHAD 51 (2015) 252–260, https://doi.org/10.1016/j.calphad.2015.10.004.

[24] H. Feufel, T. Gödecke, H.L. Lukas, F. Sommer, Investigation of the Al-Mg-Si system by experiments and thermodynamic calculations, J. Alloys Compd. 247 (1997) 31–42, https://doi.org/10.1016/S0925-8388(96)02655-2.

[25] B. Hallstedt, J. Gröbner, M. Hampl, R. Schmid-Fetzer, Calorimetric measurements and assessment of the binary Cu–Si and ternary Al–Cu–Si phase diagrams, CALPHAD 53 (2016) 25–38, https://doi.org/10.1016/j.calphad.2016.03.002.